Latest developments in micro-X-ray fluorescence (μXRF) analysis in geosciences: high-resolution element mapping, digital image analysis, and quantifications

Kaskes, Pim; Dehais, Thomas; De Graaff, Sietze Jan; Goderis, Steven; Claeys, Philippe

Published in:
Latest developments in micro-X-ray fluorescence (μXRF) analysis in geosciences: high-resolution element mapping, digital image analysis, and quantifications

Publication date:
2021

Document Version:
Final published version

Latest developments in micro-X-ray fluorescence (μXRF) analysis in geosciences: high-resolution element mapping, digital image analysis, and quantifications

Pim KASKES[1,2], Thomas DÉHAIS[1,2], Sietze J. DE GRAAFF[1,2], Steven GODERIS[1], Philippe CLAEYS[1]

[1] *Analytical, Environmental & Geo-Chemistry Research Unit, Vrije Universiteit Brussel, Pleinlaan 2, Brussels, Belgium*
[2] *Laboratoire G-Time, Université Libre de Bruxelles, Avenue F.D. Roosevelt 50, 1050 Brussels, Belgium*

Quantitative insights into the geochemistry and petrography of sedimentary, igneous, and metamorphic rocks are fundamental to understand their formational processes. Traditional analytical techniques used to obtain major- and trace-element data sets focus predominantly on either destructive whole-rock analysis or laboratory-intensive phase-specific micro-analysis. Here, we present micro–X-ray fluorescence (μXRF) as a state-of-the-art, time-efficient, and nondestructive alternative for major- and trace-element analysis for both small and large rock samples (up to 20 cm wide). This technique uses the principles of classical bulk X-ray fluorescence while being able to document the heterogeneous nature of a sample by applying multiple spot analyses, line scans, and high-resolution mapping of a flat sample surface. For the last five years, μXRF has been used for geological applications but on a relatively small scale in predominantly invertebrate palaeontology and carbonate sedimentology (e.g., de Winter & Claeys, 2016). New developments in for instance experimenting with spatial resolution and measurement time, the use of specific X-ray tube filters, and the incorporation of certified reference materials have opened a wide array of applications in different geoscientific fields due to the rapidly produced geochemical data sets by μXRF combined with petrographic and sedimentological data sets, that can be derived from μXRF maps.

We demonstrate the potential of μXRF analysis in geology by applying element mapping on 44 samples from the Chicxulub, Popigai, and Ries impact craters, including shocked crystalline basement, impact melt rocks, and impact melt-bearing polymict breccias (suevites). These samples were mapped under near-vacuum condition (20 mbar) using a Bruker M4 Tornado benchtop μXRF instrument at the Vrije Universiteit Brussel, by using a rhodium X-ray source with maximized energy settings, two silicon-drift detectors, and a polycapillary lens focusing the X-ray beam down to 25 μm. The μXRF mapping required limited to no sample preparation and generated high-resolution major- and trace-element maps in a matter of hours (~1 h for 8 cm^2, using an integration time of 1 ms for each 25-μm-diameter-pixel at a 25 μm spatial resolution). These chemical distribution maps can be used as qualitative multi-element maps, as semiquantitative single-element heat maps, and as a basis for a novel image analysis workflow. This workflow allows segmentation of clasts based on their geochemical composition rather than visual characteristics such as color. This way the modal abundance of major lithological components is quantified (Fig. 1), and an extensive data set of the size and shape of each clast is produced that aids in quantifying the degree of sorting of the sample (Kaskes et al., 2021). When thin sections are mapped with μXRF, a direct petrographic verification of clast and matrix types is also possible. However, one should take into account that elements heavier than Fe are not fully attenuated due to the limited thickness of the thin section (30 μm) and the corresponding μXRF maps are therefore less reliable. This image analysis method is a powerful tool to characterize impact breccias and other relatively coarse-grained lithologies, such as plutonic rocks, volcanic breccias, conglomerates, and meteorites.

Both whole-rock and clast-specific compositional data can be derived from µXRF mapping based on a manual selection of regions of interests. The quantification of the impact rocks from this study was based on the Standardless Fundamental Parameter method due to their strong heterogeneous nature. This technique is accurate for most major elements (with Na_2O–CaO being accurate within 10% compared to the results based on bulk powder techniques) but tends to overestimate most trace-element concentrations for samples thicker than 1 mm. To improve these results, matrix-specific calibration curves can be constructed using international reference materials in combination with the use of X-ray tube filters and a longer measurement time. Overall, we demonstrate that µXRF is more than only a screening tool for heterogeneous impact rocks, because it rapidly produces bulk and phase-specific geochemical data sets that are suitable for various applications within the earth sciences.

References

de Winter, N.J., and Claeys, Ph., 2017, Micro X-ray fluorescence (µXRF) line scanning on Cretaceous rudist bivalves: A new method for reproducible trace element profiles in bivalve calcite: Sedimentology 64(1), 231–251, https://doi.org/10.1111/sed.12299.

Kaskes, P., Déhais, T., de Graaff, S.J., Goderis, S., and Claeys, P., 2021, Micro–X-ray fluorescence (µXRF) analysis of proximal impactites: High-resolution element mapping, digital image analysis, and quantifications, in Reimold, W.U., and Koeberl, C., eds., Large Meteorite Impacts and Planetary Evolution VI: Geological Society of America Special Paper 550, p. 1–36, https://doi.org/10.1130/2021.2550(07)

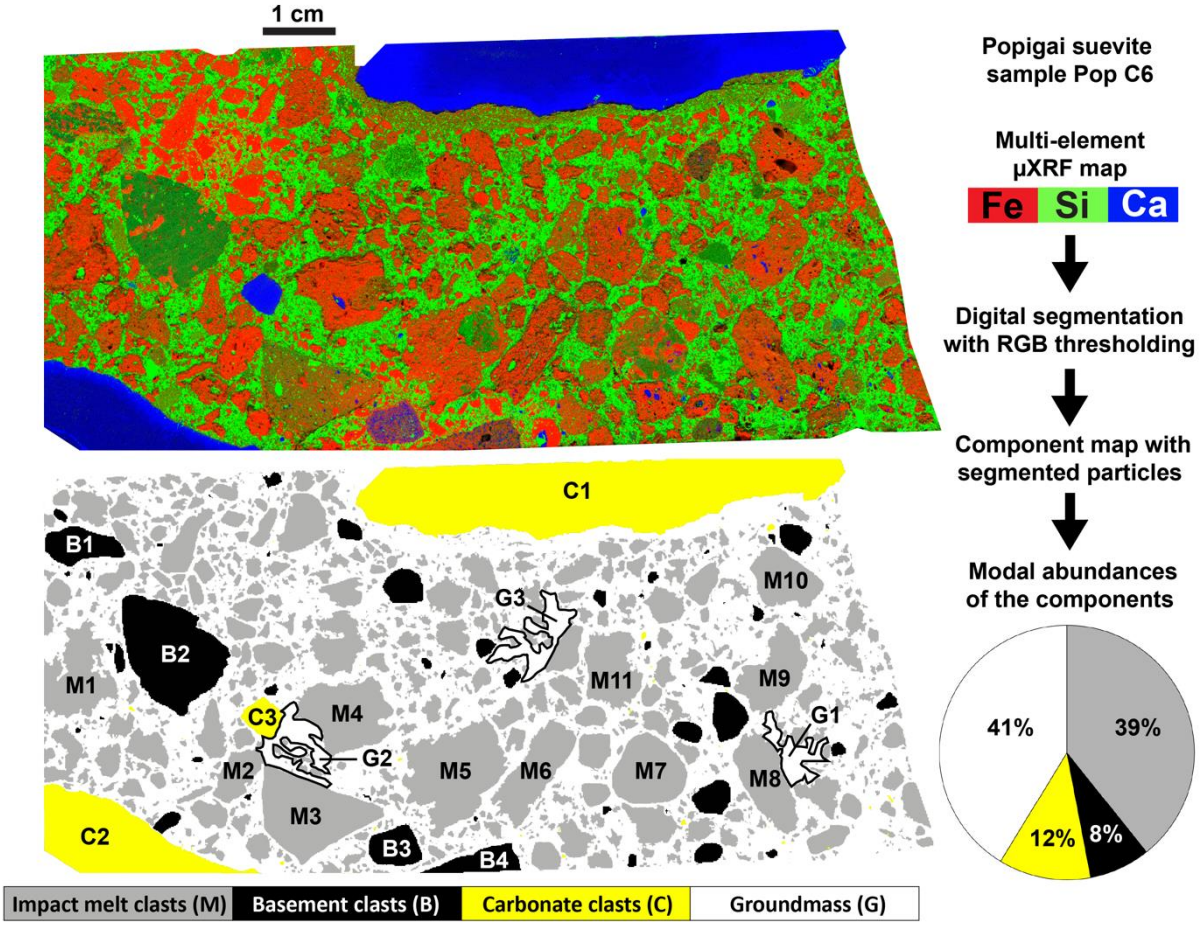

Figure 1. Image analysis results derived from digital segmentation based on an Fe-Si-Ca µXRF map from Popigai suevite sample Pop C6 (modified from Kaskes et al., 2021).